sociedade & natureza

DOI: 10.14393/SN-v32-2020-42828
Received: 15 June 2018 | Accepted: 28 May 2020

Papers

Correlation study between land use and covering with surface temperature registered by Landsat 8 satellite

Elvis Rabuske Hendges [1]
Franciele Aní Caovilla Follador [2]
Juliano Andres [3]

Keywords:
Remote sensing
TIRS sensor
Image processing
Software SPRING

Abstract
The vegetation covering of the terrestrial surface is one of the conditioning factors for the variation in air temperature found in these places. Thus, the objective of this research is to verify the spatial correlation between land use patterns and surface temperature values (Ts) recorded by Landsat 8 satellite. The study area is located in the rural area of Francisco Beltrão/PR, characterized by the presence of subsistence agricultural uses. Scene data dated 11/27/2017 and 12/13/2017 were processed, both for obtaining land use and land covering maps, as well as for surface temperature data. The registered Ts for each class of land use: water, dense forest, open forest, grazing, plantation, and cropped land showed a strong Pearson correlation, being 0.9116 and 0.9292 respectively for the mapped scenes. When analyzing the homogeneity between the Ts variances of each class, it was found that the values of the means do not have a significant minimum similarity to each other. The Tukey test showed that none of the classes of use showed similar values for the first date. For the second date, however, the water and dense forest classes had statistically similar Ts, in addition to the open forest and grazing classes.

[1] Universidade Estadual do Oeste do Paraná, Francisco Beltrão, Paraná, Brasil. e-mail: elvis_hendges@hotmail.com
[2] Universidade Estadual do Oeste do Paraná, Francisco Beltrão, Paraná, Brasil. e-mail: francaovilla@hotmail.com
[3] Universidade Estadual do Oeste do Paraná, Francisco Beltrão, Paraná, Brasil. e-mail: juliano.andres@gmail.com

INTRODUCTION

The study of the consequences of man's relationship with nature requires an understanding of the relationship between the environment and its dynamics about the physical aspects of the landscape. When man interferes in a natural environment, he alters the arrangement of physical elements that are decisive to the environmental conditions (SOARES FILHO, 1998).

One of the physical elements in the landscape is the climate. defined by a set of variables (factors and elements) that merge in time and space, revealing units that can be measured (RIBEIRO, 1993). One of the closest relationships between climatic factors and atmospheric weather conditions lies in the balance between solar radiation and vegetation, where climate elements (temperature, humidity and pressure) are the result of the radiation balance received and reflected to the atmosphere.

As a result, the relationship between the vegetation covering the terrestrial surface and the air temperature occurs by the solar radiation control (since it helps to reduce the incidence of rays on the soil) and air humidity through evapotranspiration (OLIVEIRA, 2011). According to Santos (2012), the vegetation cover, especially tree cover (through its denser foliage), absorbs most of the electromagnetic radiation from the sun (consumed in the process of photosynthesis), preventing it from reaching the surface and through its reflection heat up the nearby air layer. This fact establishes a direct relationship between the surface temperature (Ts) data and the atmospheric temperature (COELHO; RAMOS; BERGAMASCHI, 2015).

By collecting information from the reflectance of objects, Remote Sensing has excelled in mapping targets both in terms of land use and cover, climatic aspects and environmental conditions. At the orbital level, satellites and their sensors are responsible for collecting data and images, stimulating different researches in countless areas of other sciences. The Landsat 8 satellite, launched by NASA on February 11, 2013, operates at an altitude of 705 km, and it has the Operational Land Imager (OLI) sensor with 9 spectral bands and the Thermal Infrared Sensor (TIRS) sensor with 2 spectral bands in the thermal infrared, 10 bands (10.6 - 11.19 µm). The Band 10 of Landsat 8 can be used after calibration through a radiative transfer model of emissivity and parameters for recovering the surface temperature, and it has a residual polarization error of less than 2 degrees for most targets (SCHOTT et al., 2014).

In this way, information on surface temperature can be obtained by Remote Sensing because an object's internal heat is converted into radiant energy, and for most objects there is a high positive correlation between the object's true kinetic temperature and the radiant flow radiated by the object (JENSEN, 2009). Thus, it is expected that different classes of use will present different thermal behaviors, since each particularity regarding the types and intensities of covering and use of the soil reflects on environmental conditions and the balance and energy exchange relationship between the surface and the atmosphere.

Thus, this research aimed to verify the differences recorded between the Ts and the land use classes detected by the sensors of the Landsat 8 satellite in the rural area of Francisco Beltrão, State of Paraná, Brazil.

STUDY AREA

The municipality of Francisco Beltrão is situated in the southwest mesoregion of Paraná, as IBGE classification (Figure 1). According to IPARDES (2004), the southwestern mesoregion of Paraná is located, in all its territorial extension, in the Third Plateau of Paraná, which consists of basaltic spills, with sandstone sedimentary cover. The conformation of its landscape is quite uniform, determined by the shapes of small landings and plateaus. The erosive work of the rivers determined the formation of a relief of high slopes, between 25% and 50%, in certain places in the region. So, the municipality of Francisco Beltrão presents the Marrecas River as the main drainage, and it is drained by the Quatorze River, one of the main tributaries of the left margin of the Marrecas basin.

Figure 1 - Cartogram of the location of the study site in the rural area of Francisco Beltrão, State of Paraná, Brazil. location.

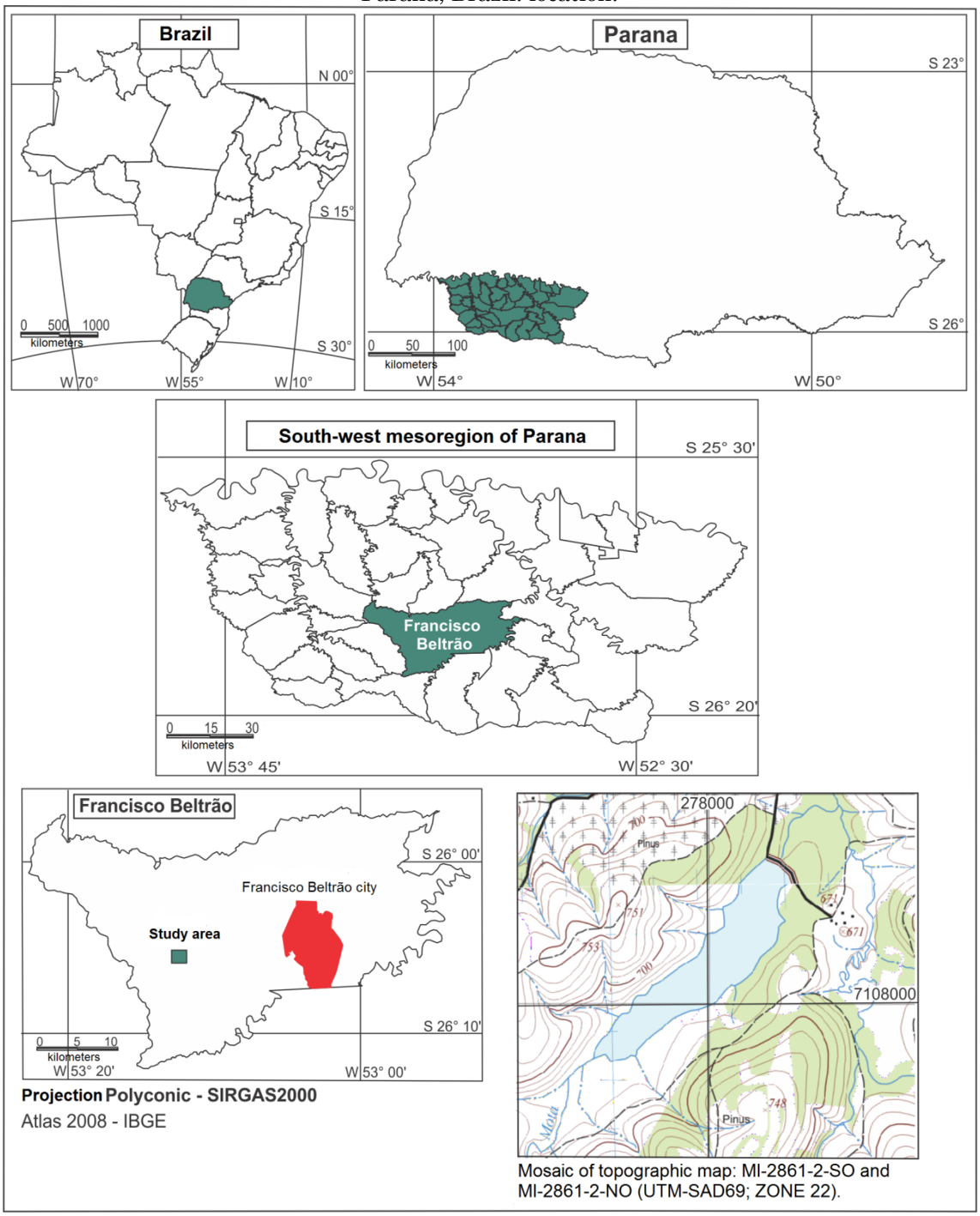

Org.: Author, 2018.

As a climatic aspect, the area presents the Subtropical Humid Mesothermal (Cfb) climate, of cool summers and winters with severe and frequent frosts. It does not have any dry season. The annual temperature averages for the hottest months are below 22°C, and for the coldest months below 18°C. Rain levels rates between 1,600 and 1,900 mm and relative humidity of 85%. Temperature and humidity are determining factors in the spatialization of native vegetation remnants characteristic of the phytogeographic domains of Mixed Ombrophilous Forest (Araucaria forest in the higher regions) and the Seasonal Semideciduous Forest, composed of subtropical species located in lower altitude areas (IPARDES, 2004).

As for human aspects, the southwest of Paraná mesoregion is marked by the intense struggle over land ownership in the 1950s, with a view to wood exploitation. Currently, subsistence

crops are the predominant land structure in the rural area of Francisco Beltrão. In the 2010 census (IBGE), the municipality counted an area of 735 km², and a population of 87,491 inhabitants is estimated for 2016 (IBGE, 2010).

MATERIALS AND METHODS

Initially, a review of concepts on orbital remote sensing and digital image processing was carried out (ARIZA, 2013; FLORENZANO, 2005, 2007; JENSEN, 2009; MOREIRA. 2005; NOVO, 1992, PONZONI; SHIMABUKURO, 2010), in addition to the use of thermal images to identify surface temperature (Ts) (COELHO; CORREA, 2013; MONTEIRO; MENDONÇA, 2003; NASCIMENTO, 2011; SOUZA; JÚNIOR, 2012).

Landsat 8 images were used as data sources. From the OLI sensor, for mapping land use. And the TIRS sensor with thermal infrared images . (ARIZA, 2013). The Landsat 8 satellite scenes, dated November 27, 2017 and December 13, 2017, were acquired from of the United States Geological Survey (USGS) website (https://landsat.usgs.gov/landsat-data-access). The products/images characteristics are consistent with the Level 1 standard (orthorectified). The data format provided is a TXT (metadata) and GeoTIFFs in a compressed file about 1 GB (compressed) to 2 GB (uncompressed). The radiometric resolution is 16 Bits, Datum WGS 1984, UTM projection (COELHO; CORREA 2013). Thus, the images were imported into a Geographic Database delimited by coordinates representative of the study area. The spectral bands 1, 2, 3, 4, 5, 6, and 7 of the OLI sensor were used to perform automated pixel classification, transforming the digital number (DN) of the spectral record of the images into a land use theme. According to Novo (1992), the interaction of energy is the main tool for the study of remote sensing, as it is through the different response patterns of interactions that an object can be identified on the Earth's surface.

To reduce the image classification matrix confusion, six classes of land use were defined: water, dense forest, open forest, grazing, plantation (agricultural areas in the initial stage of plant growth, due to the period studied) and cropped land (agricultural areas in preparation for planting). Vegetation reflectance is determined by several factors such as leaf geometry, plant morphology, physiology and chemistry (PONZONI; SHIMABUKURO, 2010). These factors, related to the sunlight angle of incidence, allow digital image processing techniques to differentiate plant species in extracts. (MOREIRA, 2005). The spectral behavior of rocks and exposed soil elements, on the other hand, is quite similar, which helps the grouping of their spectral responses in a class (JENSEN, 2009).

The image classification was performed in the SPRING software (Georeferenced Information Processing System) using the histogram classifier, which is an iterative grouping algorithm that classifies segmented regions in a certain pre-defined number of classes automatically from the covariance average and matrix (MOREIRA, 2011).

The confidence level of the classified image was obtained through a confusion matrix to verify the errors arising from the process of assigning pixels to certain classes. This matrix will use a grid of sampling points randomly distributed and significant to the classified area. Equation 01 formulates the sample size determination (n) based on the estimate population average (area size).

$$n = \frac{N.\sigma^2.\left(Z_{\frac{\alpha}{2}}\right)^2}{(N-1).(E)^2 + \sigma^2.\left(Z_{\frac{\alpha}{2}}\right)^2} \qquad 1$$

Where:
n= Number of samples.
N = Population size.
σ= Population standard deviation of the studied variable.
Zα/2 = Critical value that corresponds to the desired confidence degree.
E = Margin of error or estimate maximum error.

With the spatial distribution of the sample points, confusion matrices generated from the revalidation of the classification were elaborated. The classified pixels will be compared with images of very high spatial resolution images (up to 0.5 m) from the Pléiades 1A satellite (developed by the French space agency, CNES), made available by the Google Earth software. Mapping approach developed by Moreira (2011), which uses high spatial resolution images captured from Google Earth as a basis and visual interpretation technique described by Novo (2008).

The accuracy assessment was based on Congalton (1991), through the calculation of the Kappa coefficient, which takes into account the entire confusion matrix, including the elements outside the main diagonal. The performance levels according to the Kappa index are: < 0 = very

poor; 0 - 0.2 = bad; 0.2 - 0.4 = reasonable; 0.4 - 0.6 = good; 0.6 - 0.8 = very good; and 0.8 - 1.0 = excellent. To calculate the Kappa coefficient, Equation 2 was used:

$$K = \frac{n \sum_{i-1}^{c} x_{ii} - \sum_{i-1}^{c} x_{i+} x_{+i}}{n^2 - \sum_{i-1}^{c} x_{i+} x_{+i}} \quad 2$$

Onde:
k= Kappa coefficient.
n = total samples.
$\sum_{i-1}^{c} x_{ii}$= sum of the main diagonal of the error matrix.
$\sum_{i-1}^{c} x_{i+} x_{+i}$= sum of the product of the rows and columns of the error matrix.

For the Ts mapping, Schott et al. (2014), point out that the thermal images of Landsat 8 band 10 use is recommended only after calibration using atmospheric correction models and parameters for Ts recovery, but a residual polarization error of less than 2 degrees is still recognized for the targets. (SCHOTT et al. 2014).

For the scenes atmospheric correction model of the thermal sensor TIRS, it was first necessary to perform the air transmissivity calculation values and the radiance emitted and radiance received by the surface. For such a procedure, it was necessary to inform data from a local weather station (Table 1), such as local air temperature, atmospheric pressure, and humidity at the time of image recording.

Table 1: Atmospheric correction model data applied to the images.

Data	11:30 am – November 17, 2017	11:30 am – December 13, 2017
Air temperature[1]	22.2 °C	24.5 °C
Atmospheric pressure[1]	939.7 hPa	941.91 hPa
Relative air humidity[1]	68%	65%
Atmospheric transmissivity[2]	0.84 K	0.82 K
Emitted Radiance[2]	1.31 W/m².sr. µm	1.53 W/m².sr. µm
Received Radiance[2]	2.16 W/m².sr. µm	2.51 W/m².sr. µm

Source: 1SIMEPAR data (Paraná Meteorological System) for the study area; [2] values calculation performed by the NASA website http://atmcorr.gsfc.nasa.gov./. Org.: Author, 2018.

Thus, with the data of atmospheric transmissivity (0.86 K), radiance emitted (1.10 W/m².sr.µm) and received (1.88 W/m².sr.µm) by the surface, through the Equation 03 (BARSI, 2003), it was possible to calculate the radiance (Lt).

$$Lt = \frac{L_{TOA} - L_u - (1-\varepsilon) . L_d}{\tau . \varepsilon} \quad 3$$

Onde:
Lt= Radiance of a black target of kinetic temperature (W/m².sr.µm).
L_{TOA} = Spectral radiance (W/m².sr.µm).
τ = Atmospheric transmissivity.
ε= Surface emissivity.
Lu = Radiance emitted by the surface (W/m².sr.µm).
Ld = Radiance received by the surface (W/m².sr.µm).

As an input parameter, corresponding to emissivity, it was decided to use the value of 0.935 K, which corresponds to the average value between surfaces without vegetation (0.92 K) and areas with vegetation (0.95 K) (NICHOL, 1994). Thus, after the atmospheric correction, it was necessary to perform the Ts calculation for LANDSAT 8 from the gray levels conversion of the band 10 in spectral radiance using Equation 04 (USGS, 2014). With the calculation performed, the resulting Ts values were also converted to Degree Celsius (°C) with the subtraction of the temperature value of the water freezing point at sea level, which is equivalent to 273.15°Kelvin.

$$L_\lambda = M_L . Q_{cal} + A_L \quad 4$$

Onde:
Lλ= Spectral radiance (W/m².sr.µm).
M_L = Multiplying factor for resizing the band (3,3420 . e^{-4}).
Q_{cal} = Quantized and calibrated gray pixel value (DN).
A_L = Resizing additive factor for the band (0,1).

The calculations defined by the mathematical equations mentioned above, as well as the processes of spatial information crossing between the land use maps and the registered Ts, were carried out through map algebra, implemented with the code Spatial Language for Algebraic Geoprocessing (LEGAL), in the SPRING software.

To verify if the values related to Ts recorded by the OLI sensor are consistent with the terrestrial reality found, field incursions were

carried out on the dates and time of the satellite's passage through the imaged location, where the water temperatures were collected through a heat sensor. It is known that the studies of physical-chemical parameters of water, especially of temperature, are the result of solar radiation on water. The temperature differences generate water layers with different densities forming a physical barrier that prevents them from mixing, and when the wind energy is not enough to mix them, the heat is not evenly distributed in the water column, creating thus homogeneous thermal strata (ESTEVES, 1998).

To compare whether the water temperature data measured in the field are similar to the Ts recorded by the satellite, the statistical test calculation of the signals from related samples was performed. The test of the signals (non-parametric) is applied in situations where the researcher wants to determine if two conditions are different.

To verify statistically whether the land use and land covering factor influences the climatic element of Ts, information from each of the six classes of use was crossed, an external strip of 30m was extracted aiming to reduce the influence of regions characterized by other adjacent uses.

The aforementioned crossing originated data for calculating Pearson's correlation. Pearson's linear correlation coefficient, according to Turkman and Silva (2000), establishes a correlative measure parameter that establishes a level of intensity of the relationships between the variables. The results in this coefficient present values in the range of -1 to 1. It is understood as a perfect negative correlation (variables do not have any type of relationship) if the value obtained is -1. If the result of the coefficient shows a value of 1, the relationship between the variables is perfectly direct. For intermediate values the authors indicate the following analyzes between the ranges of values: 0.01 to 0.39 the correlation is weak; 0.40 to 0.69 the correlation is medium; and 0.70 to 0.99 the correlation is strong.

In addition to Pearson's correlation, Tukey's statistical test and analysis of variance (ANOVA) were also used to confirm whether Ts mapped to each of the land use and land covering classes have a difference in their mean.

RESULTS AND DISCUSSION

After the database creation in the SPRING software, the LANDSAT 8 satellite images were imported. Figure 2 presents the image cards in a false color combination between bands 7, 5, and 4 (RGB) and the maps of land use and covering arising from the classification.

Numerous areas classified as cropped land (magenta and pink shades) for an image dated November 27th, 2017 evolved to the plantation class (changing the color) in the image of December 13th, 2017. This is because the region is characterized by annual crops (e.g. soybeans and corn), and soybean crops were in an initial growth phase.

When performing the bands' classification, the class of water and dense forest and open forest, which together represented 53% of the study area, showed great area similarity for the mapped dates. The class plantation, on the other hand, showed an increase of 38 ha (445%), mainly at the expense of decreasing cropped land areas (-23 ha) and grazing (-12 ha) plus 3 ha of reduced open forest.

After the classification was done, the calculation which defined the 60 sample points (10 for each class) was carried out using 95% of value for the confidence degree and 5% as the error margin. Thus, the random grid estimated an average distance between sample points of 170 m for latitude and 330 m for longitude (6 columns with 10 points each).

After the classified images were compared (land use maps) with the image provided by Google Earth dated July 1st, 2016, at the predefined sampling points, a confusion matrix was generated allowing the calculation of Kappa coefficient to analyze the degree of reliability of the ratings of both scenes. This calculation resulted in values of 0.7692 for the first image and 0.7507 for the second image, both values framed in a very good level of classification.

The image referring to band 10 of the TIRS sensor, after being subjected to atmospheric correction and transformed to Ts values in degrees Celsius, showed a variation between 21 to 34 °C (11/27/2017) and from 23 to 36°C (12/13/2017).

The pixel present in the image quantifies the average Ts recorded by the sensor according to the reflectance of the targets distributed on the Earth's surface, which is in turn different from the air temperature measured by the weather stations.

Figure 2 - Maps and image cards of land use and cover.

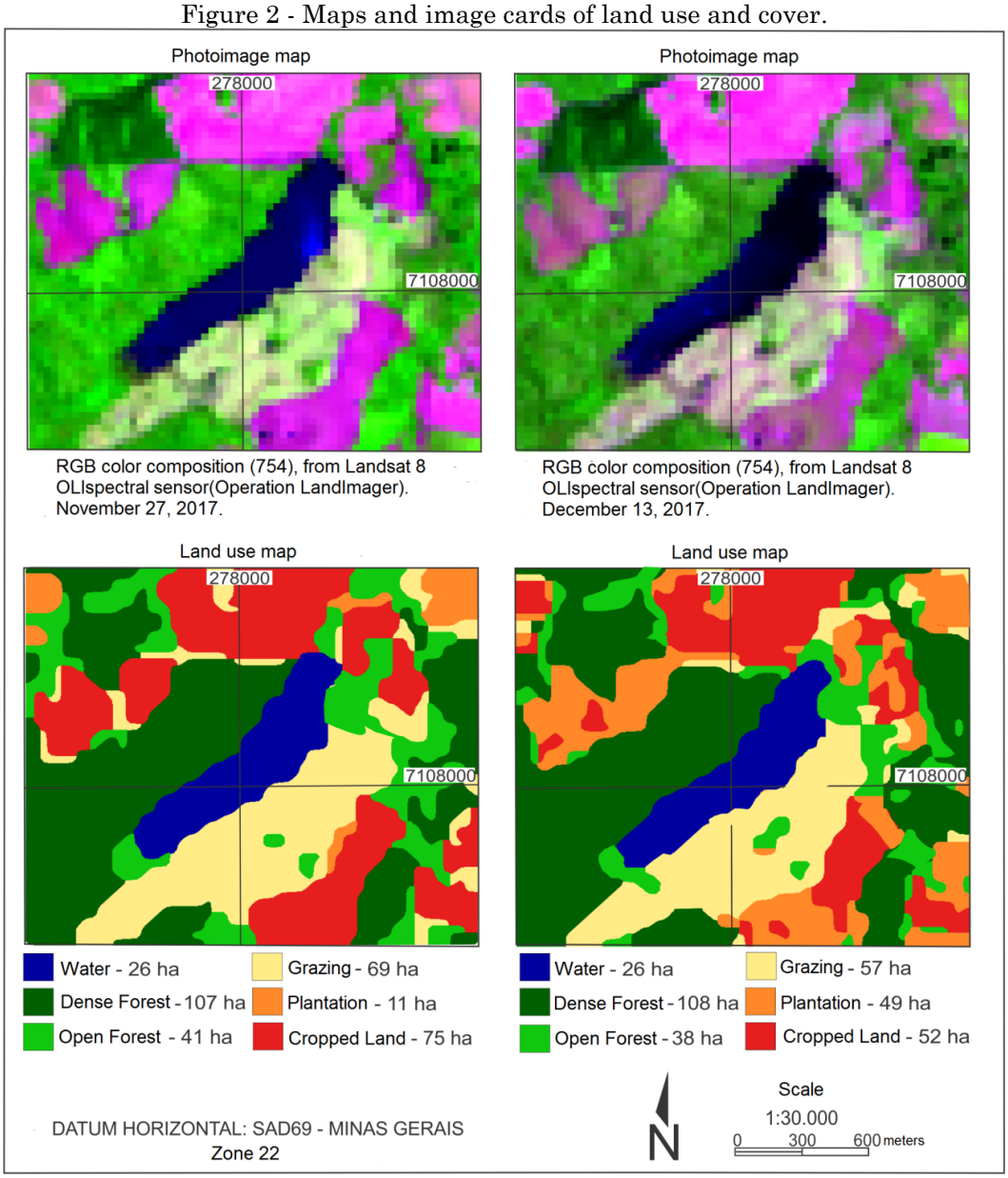

Org.: Author, 2018.

Thus, Weng, Lu and Schubring (2004); and Coelho, Ramos and Bergamaschi (2015), in their studies emphasize that the average surface temperature normally presents higher values concerning the average air temperature. However this difference does not interfere in the results because the temperature quantified by the satellite is the surface radiant temperature.

To check the information from the TIRS sensor, the Ts were compared with the temperature values measured in the site (Table 2), by the statistical test of the signals where a non-significant difference, once p=0.096 for 5% significance limit (p≥0,05).

When correlating the data of the Ts and land use and covering maps, the Ts values of each pixel of each class of use and covering were mapped and compared by the value of the average temperature of each class, extracted from the marginal range of 30m. Thus, Pearson's correlation value showed positive values of 0.91 (strong correlation) for 11/27/2017, with the water and plantation class representing a lower variance of their temperatures concerning the average temperature of their class (s=0.34 and 0.56 respectively).

Table 02 - Temperature values verified in the field and Ts recorded by the satellite.

Point / Location	November 17, 2017		December 13, 2017	
	Site (°C)	TIRS (°C)	Site (°C)	TIRS (°C)
P1 (W53°13'2"; S26°07'36")	22	23.01	26	26.15
P2 (W53°13'9"; S26°07'47")	23	23.24	26	25.84
P3 (W53°13'19"; S26°07'52")	23	23.01	25	25.33
P4 (W53°13'8"; S26°07'35")	24	23.75	25	24.88
P5 (W53°13'15"; S26 07'44")	24	23.53	25	24.64
P6 (W53°13'24"; S26°07'50")	24	23.42	25	24.59
P7 (W53°13'22"; S26°07:51")	24	23.52	25	24.55
P8 (W53°13'12"; S26°07'45")	25	24.88	25	24.60
P9 (W53°13'5"; S26°07'35")	25	24.58	26	25.24

Org.: Autor, 2018.

This factor can be explained by the homogeneous extract, both for the surfaces of water depths and for agricultural crops in initial growth stage. The class of open forest, composed of different plant extracts (ground level, shrub and tree), showed a greater variation in temperatures (s=1.64), followed by the class of cropped land with a standard deviation of s=1.15 (Figure 3).

Figure 3 - Scatter diagram of the Ts of the classes of use X Average Ts of each class of use for the date of November 17, 2017.

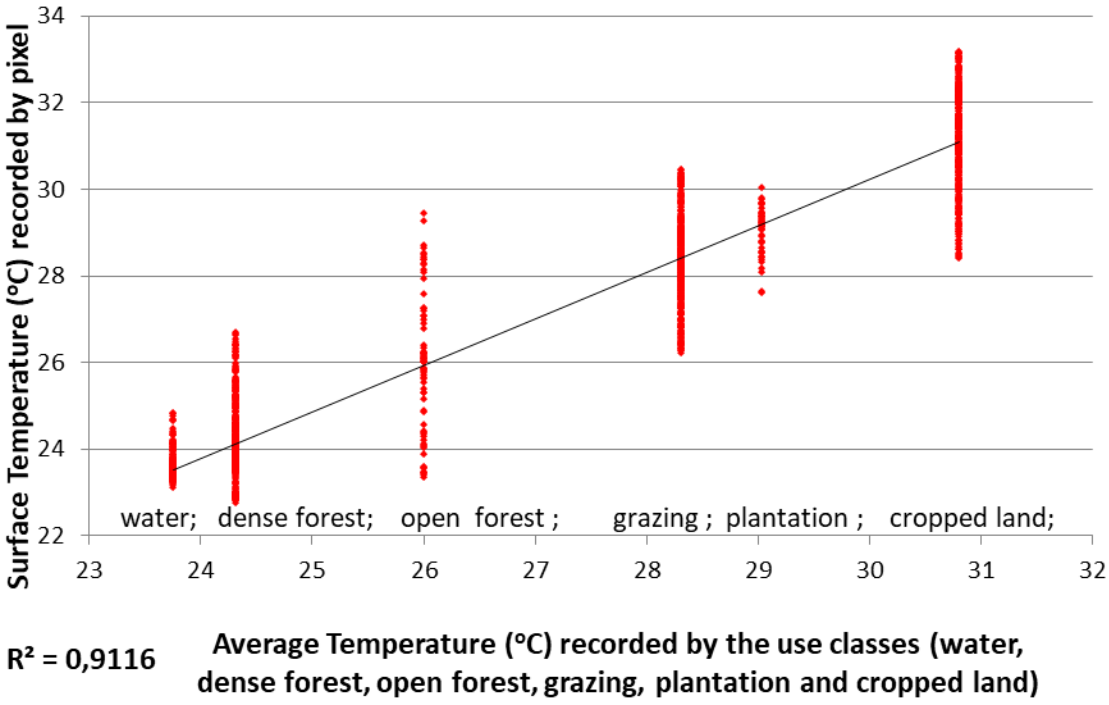

Org.: Author, 2018.

With higher temperature averages as well as representative Ts for each pixel mapped in the land use and land covering classes, the date of 12/13/2017 also presented a strong statistical correlation of Pearson (0.93). cropped land class presented some low temperatures concerning its average, leaving this class with the highest standard deviation between the measured Ts and the general class average (s=1.41). This factor can be explained by humidity or by soil recently moved by agricultural activities (Figure 4). The water class was had the lowest standard deviation for that date (s=0.47).

Figure 4 - Scatter diagram of the Ts of the classes of use X Average of each class of use for the date of December 13, 2017.

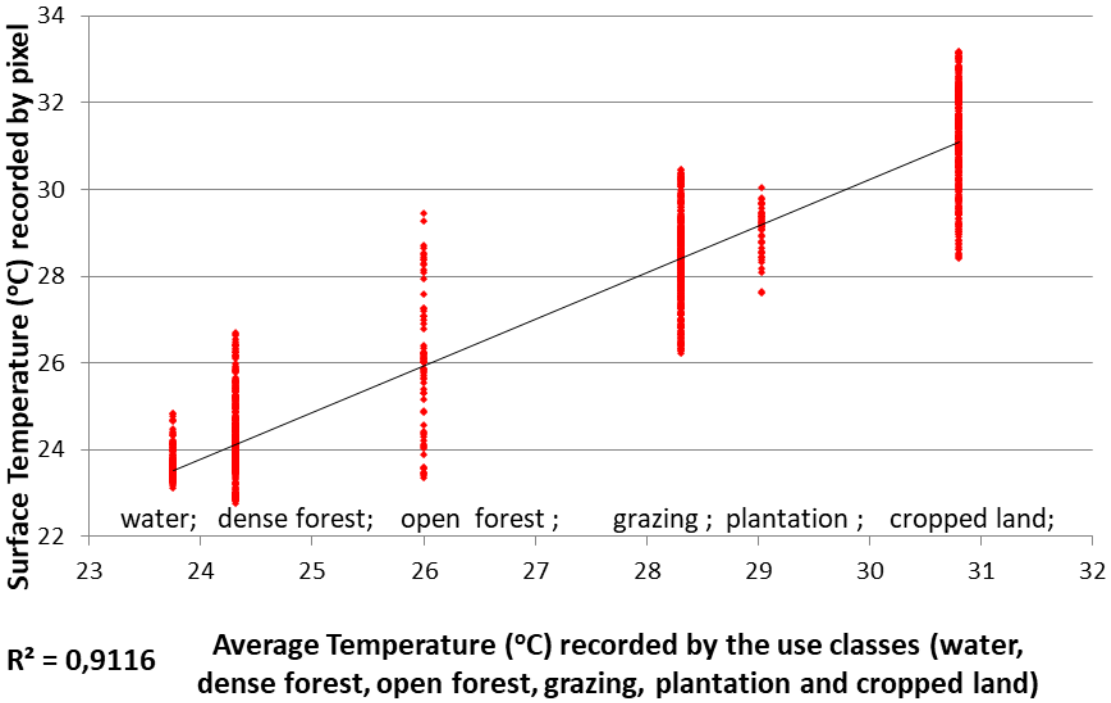

Org.: Author, 2018.

It can also be seen in figures 3 and 4 subtracting the water class, there is an inversely proportional tendency between Ts and the plant extract, that is, as the Ts average increases, a decrease in the plant extract is identified.

When analyzing the homogeneity between the variances (ANOVA) for the Ts values of each of the groups of land use and covering on the dates studied, the calculated F presented the values of Fcal = 3,593,199 (November 27, 2017) and of Fcal = 4,516,345 (December 13, 2017), with $p < 0.001$. To demonstrate which use classes differ from each other, or which classes can be grouped by similarities of registered Ts, the Tukey test indicated that for the first date (11/27/2017) none of the use classes presented similar values to each other. For the second date 11/13/2017, however, the water and dense forest classes showed statistically similar Ts (0.252), in addition to the classes of open forest and grazing (0.899).

FINAL CONSIDERATIONS

Through this research it was possible to recognize that the Ts registered by the OLI sensor, as well as the different thermal sensations observed in the rural area of Francisco Beltrão, have a direct relationship with the mapped land use patterns, mainly taking into account the prevailing vegetation patterns. It is recommended to conduct further studies with sensors capable of operating at different spectral resolutions with thermal infrared length, as well as with greater spatial resolutions, due to the wide variety in the mosaic of uses found in the study area.

REFERÊNCIAS

ARIZA, A. **Description y Correccion de Productos Landsat 8**. Instituto Geográfico Agustin Codazzi, Bogotá, 2013.

BARSI, J. A.; BARKER, J. L.; SCHOTT, J. R. An atmospheric correction parameter calculator for a single thermal band earth-sensing instrument. In: **Geoscience and Remote Sensing Symposium**. Toulouse, p. 3014-3016, 2003.

COELHO, A. L. N.; RAMOS, A. L. D.; BERGAMASCHI, R. B. Aplicação dos Produtos Landsat-8/TIRS/OLI e Aster/GDEM na Avaliação do Comportamento Termal de Superfície, Usos e Topografia. **XVII Simpósio Brasileiro de Sensoriamento Remoto – SBSR**. João Pessoa, p. 1323-1330, 2015.

COLGATON, R. G. A review of assessing the accuracy of classifications of remotely sensed data. **Remote Sensing of Environment** , v. 49, n. 12, p. 1671-1678, 1991.

ESTEVES, F. A. **Fundamentos da Limnologia**. 2ª Ed Interciência Rio de Janeiro. 1998. 602 p.

FLORENZANO, T. G. **Iniciação em Sensoriamento Remoto**: Imagens de satélites para estudos ambientais. 2ª Ed. Oficina de Textos, São Paulo, 2007.

FLORENZANO, T. G. Geotecnologias na Geografia Aplicada: difusão e acesso, **Revista do Departamento de Geografia**, USP no 17, p. 24 – 29. 2005. https://doi.org/10.7154/RDG.2005.0017.0002.

IBGE. Instituto Brasileiro de Geografia e Estatística. **Base de Informações do Censo Demográfico 2010**: resultados do universo por setor censitário - documentação do arquivo. Rio de Janeiro: IBGE, 2011, 201 p.

IPARDES, Instituto Paranaense de Desenvolvimento Econômico e Social. **Leituras regionais**: Mesorregião Sudoeste Paranaense. Curitiba, BRDE, 2004, 139 p.

JENSEN, J. R. **Sensoriamento Remoto do Ambiente**: uma perspectiva em Recursos Terrestres. Traduação de José Carlos Neves Epiphanio. São José dos Campos, SP: Parênteses, 2009. 598 p.

MONTEIRO, C. A. de F.; MENDONÇA, F. **Clima urbano**. São Paulo. Contexto. 2003

MOREIRA, M.; A. **Fundamentos do Sensoriamento Remoto e metodologias de aplicação**. 3a edição. Viçosa: UFV. 3a edição. 2005.

MOREIRA, M. A. Uso de imagens do Google Earth capturadas através do software stitch map e do TM/Ladsat-5 para mapeamento de lavouras cafeeiras – nova abordagem metodológica. **XV Simpósio Brasileiro de Sensoriamento Remoto**. Curitiba, p. 481-488. 2011.

NASCIMENTO, I. J. de. **Emprego de técnicas de sensoriamento remoto e de geoprocessamento na análise multitemporal do fenômeno de ilhas de calor no município de Goiânia-GO** (1986/2010). 96f. Dissertação (Mestrado em Geografia) – Universidade Federal de Goiás, Goiânia, 2011.

NICHOL, J. E. A GIS-Based Approach to Microclimate Monitoring in Singapore's High-Rise Housing Estates. **Photogrammetric Engineering & Remote Sensing**, v.60, n. 10, p. 1225-1232, 1994.

NOVO, E. M. L. de M. **Sensoriamento remoto**: princípios e aplicações. 3a edição. São Paulo, Edgard Blucher, 2008.

OLIVEIRA, A. S. **Influência da vegetação arbórea no microclima e uso de praças públicas**. Cuiabá, 2011.

PONZONI, F. J.; Shimabukuro, Y. E. **Sensoriamento Remoto no Estudo da Vegetação**. Editora Parêntese, São Paulo. 2010.

RIBEIRO, A. G. As Escalas do clima. **Boletim de Geografia Teorética**, Rio Claro, v. 23, p. 288-294, 1993.

SANTOS, J. S. dos. Campo térmico urbano e sua relação com o uso e cobertura do solo em cidade tropical úmida. **Revista Brasileira de Geografia Física**, Recife, v. 03, p. 540-557, 2012. https://doi.org/10.26848/rbgf.v5i3.232851.

SCHOTT, J. R.; GERACE, A.; RAQUENO, N.; IENTILUCCI E.; RAQUENO, R.; LUNSFORD, A. W. Chasing the TIRS ghosts: calibrating the Landsat 8 thermal bands, **Earth Observing Systems XIX**, Califórnia, v. 9218, p. A1 - A20, 2014. https://doi.org/10.1117/12.2063236

SOARES FILHO, B. S. **Modelagem da dinâmica da paisagem de uma região de fronteira de colonização amazônica.** 299f. Tese (Doutorado), Escola Politécnica, Universidade de São Paulo. São Paulo, 1998.

SOUZA, S. B. de; JÚNIOR, L. G. F. Relação entre temperatura de superfície terrestre, índices espectrais e classes de cobertura da terra no município de Goiânia (GO). **Revista Espaço Geográfico** em Análise. Vol. 26. Paraná, p. 75-99. 2012. https://doi.org/10.5380/raega.v26i0.30151.

TURKMAN, M. A.; SILVA, G. L. **Modelos Lineares Generalizados - da teoria à prática**. Sociedade Portuguesa de Estatística, Lisboa. 2000.

USGS (United States Geological Survey). **Using the USGS Landsat 8 Product**. Disponível em: https://landsat.usgs.gov/Landsat8_Using_Product.php .Acesso em: 29.out.2014.

WENG, Q.; LU, D.; SHUBRING, J. Estimation of land surface temperature–vegetation abundance relationship for urban heat island studies. **Remote Sensing of Environment**. n. 89, p. 467-483, 2004. https://doi.org/10.1016/j.rse.2003.11.005